Received: 19 April 2022 | Revised: 2 November 2022 | Accepted: 12 November 2022

DOI: 10.1002/hbm.26160

RESEARCH ARTICLE

WILEY

Detailed anatomic segmentations of a fetal brain diffusion tensor imaging atlas between 23 and 30 weeks of gestation

Camilo Calixto[1,2] | Fedel Machado-Rivas[1,2] | Davood Karimi[1,2] | Maria C. Cortes-Albornoz[1,2] | Lina M. Acosta-Buitrago[4] | Sebastian Gallo-Bernal[2,3] | Onur Afacan[1,2] | Simon K. Warfield[1,2] | Ali Gholipour[1,2] | Camilo Jaimes[1,2]

[1]Computational Radiology Laboratory, Department of Radiology, Boston Children's Hospital, Boston, Massachusetts, USA

[2]Harvard Medical School, Boston, Massachusetts, USA

[3]Massachusetts General Hospital, Boston, Massachusetts, USA

[4]Universidad del Rosario School of Medicine, Bogotá, Colombia

Correspondence
Camilo Jaimes, Boston Children's Hospital, Department of Radiology, 55 Fruit Street, 2nd floor Main Building, Boston, MA 02215, USA.
Email: camilo.jaimescobos@childrens.harvard.edu

Funding information
American Roentgen Ray Society Scholarship; Career development award from the Office of Faculty Development at Boston Children's Hospital; Technological Innovations in Neuroscience Award from the McKnight Foundation; National Institute of Neurological Disorders and Stroke, Grant/Award Numbers: R01EB013248, R01EB018988, R01EB031849, R01EB032366, R01HD109395, R01NS106030, R01NS121657; NIH Office of the Director, Grant/Award Number: S10OD0250111; Rosamund Stone Zander Translational Neuroscience Center, Boston Children's Hospital; National Institute of Biomedical Imaging and Bioengineering; Eunice Kennedy Shriver National Institute of Child Health

Abstract

This work presents detailed anatomic labels for a spatiotemporal atlas of fetal brain Diffusion Tensor Imaging (DTI) between 23 and 30 weeks of post-conceptional age. Additionally, we examined developmental trajectories in fractional anisotropy (FA) and mean diffusivity (MD) across gestational ages (GA). We performed manual segmentations on a fetal brain DTI atlas. We labeled 14 regions of interest (ROIs): cortical plate (CP), subplate (SP), Intermediate zone-subventricular zone-ventricular zone (IZ/SVZ/VZ), Ganglionic Eminence (GE), anterior and posterior limbs of the internal capsule (ALIC, PLIC), genu (GCC), body (BCC), and splenium (SCC) of the corpus callosum (CC), hippocampus, lentiform Nucleus, thalamus, brainstem, and cerebellum. A series of linear regressions were used to assess GA as a predictor of FA and MD for each ROI. The combination of MD and FA allowed the identification of all ROIs. Increasing GA was significantly associated with decreasing FA in the CP, SP, IZ/SVZ/IZ, GE, ALIC, hippocampus, and BCC ($p < .03$, for all), and with increasing FA in the PLIC and SCC ($p < .002$, for both). Increasing GA was significantly associated with increasing MD in the CP, SP, IZ/SVZ/IZ, GE, ALIC, and CC ($p < .03$, for all). We developed a set of expert-annotated labels for a DTI spatiotemporal atlas of the fetal brain and presented a pilot analysis of developmental changes in cerebral microstructure between 23 and 30 weeks of GA.

KEYWORDS
atlas, diffusion, fetal MRI, microstructure, segmentation

1 | INTRODUCTION

Fetal life is characterized by a dynamic sequence of neurodevelopmental events. During this period, the brain undergoes exponential growth, neurons reach their cortical and subcortical targets, myelination begins, and transient zones in the telencephalic wall evolve and give rise to the mature cerebral hemispheres (Kostović et al., 2019). The potential of utilizing diffusion tensor imaging (DTI) to investigate

these intricate cytoarchitectonic and myeloarchitectonic changes in vivo is enormous (Neil et al., 1998). However, challenges related to the developmental anatomy of the fetuses, constant subject motion, and lack of robust computational neuroimaging tools for the analysis of fetal DTI have historically hindered these analyses.

Most data on brain DTI before 40 weeks of post-conceptional age emanates from ex vivo (Feng et al., 2019; Gupta et al., 2005; Huang et al., 2009; Trivedi, Husain, et al., 2009; Widjaja et al., 2010) and preterm infant (Maas et al., 2004; McKinstry, 2002) MRIs. While these data contribute immensely to our understanding of prenatal brain development, generalization of these observations is difficult due to technical and biological differences. For example, the resolution of images acquired ex vivo exceeds that of in vivo DTI by almost an order of magnitude (Huang et al., 2009), and the effects of preterm birth cannot be controlled for (Batalle et al., 2017; Nosarti et al., 2014). Furthermore, the period between 20 and 30 weeks post-conceptional age is sparsely sampled in these studies, creating a critical gap. This period represents the time at which most clinical fetal MRIs are obtained (Manganaro et al., 2017). It also includes the currently accepted limit of preterm birth viability, at approximately 24 weeks of postconceptional age, which is followed by a period of heightened vulnerability to brain injury as exemplified by the elevated risk of neurodevelopmental disability in infants born in this later stage of the second trimester (Woodward et al., 2006).

Recent developments in fetal image processing techniques stand to close this technical gap and facilitate in utero analysis. In particular, the development of robust fetal DTI motion correction algorithms (Marami et al., 2017) and the creation of spatiotemporal atlases of fetal brain DTI (Khan et al., 2019) lay the foundation for constructing analytic tools specific to the developmental stage of the subjects being studied. The missing element required to perform anatomy-specific analyses, analogous to those in newborns and adults, is the creation of regions of interest (ROI) in the diffusion space. While detailed segmentation algorithms exist for structural data based on T2-weighted super-resolution reconstructions, the differences in tissue contrast and distortions with the DTI sequences preclude their utilization For example, in fetal MRI, there is a high likelihood of significant motion between DWI and T2-weighted structural acquisitions. In addition, geometric distortions due to susceptibility-induced B1 field inhomogeneities can affect echo-planar imaging, which is used in fetal DWI. These distortions can lead to deformations and signal loss that can significantly reduce the accuracy of T2 to DWI registration (Huang et al., 2008).

This work aimed to create detailed anatomic labels for a fetal brain DTI spatiotemporal atlas between 23 and 30 weeks of post-conceptional age. We focused on younger gestational ages (GA) as their developmental neuroanatomy differs the most from the existing tools for analyzing neonatal brain DTI (Bastiani et al., 2019; Oishi et al., 2011), which correlates with the presence of the readily visible transient fetal zones (Maas et al., 2004). We hypothesize that the mean diffusivity (MD) and fractional anisotropy (FA) maps from the spatiotemporal atlas will allow sufficient contrast for the accurate segmentation of structures. Our study enables a pilot analysis of microstructural changes within individual regions of the fetal brain. Furthermore, we utilized a tensor-to-tensor registration algorithm to propagate the labels from the atlas to DTI of individual fetuses, demonstrating the feasibility of atlas-based regional fetal brain DTI analyses.

2 | MATERIALS AND METHODS

2.1 | Diffusion atlas

We performed detailed anatomic segmentations on a publicly available spatiotemporal DTI atlas of fetal brain development (http://crl.med.harvard.edu/research/fetal_brain_atlas/) (Khan et al., 2019). The subjects for the original study consisted of 60 pregnant women prospectively recruited as part of a HIPAA-compliant IRB-approved study. The women for that study were healthy controls between 18 and 45 years, with no significant comorbidities and normal prenatal exams. Women with the following criteria were included: (1) no contraindication for MRI, (2) no known history of fetus congenital infection, (3) no fetal brain or other physical abnormalities, (4) no chromosomal abnormalities, (5) single pregnancy, and (6) no known genetic disorders of parents or siblings.

All MRIs were acquired using a Siemens MAGNETOM Skyra 3T MRI scanner with a 16-channel body matrix and spine coils. The study utilized a series of orthogonal 12-direction DTI acquisitions with a maximum b-value of $b = 500\ \mathrm{s/mm^2}$; a motion-tracked slice-to-volume registration (MT-SVR) was utilized for motion-robust data processing and image reconstruction (Marami et al., 2017). Subsequently, the authors computed a series of spatiotemporal atlases at 1-week intervals, utilizing between 9 and 13 subjects for each week (Table 1S) with a truncated-Gaussian kernel with a flexible bandwidth. Then, a Nadaraya-Watson kernel regression was used to compute a representative atlas for each GA (Khan et al., 2019).

2.2 | Segmentations

We performed segmentations based on the FA and MD atlases corresponding to GA 23–30. All segmentations were performed in ITK-SNAP (version 3.8.0) using a high-resolution (1080p) Wacom® Cintiq tablet. Two research fellows (*Camilo Calixto*, MD and *Maria Cortes-Albornoz*, MD) performed the segmentations, and a board-certified neuroradiologist with fellowship training in pediatric neuroradiology (*Camilo Jaimes*, with 5 years of experience in fetal imaging) revised them as needed. The segmentations were outlined primarily on the FA maps as they offer inherently high tissue contrast (high anisotropy) in the fetal cortex and fiber-rich white matter regions (e.g., corpus callosum, internal capsule, external capsule). The color-coded FA (cFA) maps were utilized to aid in identifying structures with coherent architecture (high FA) and distinct direction of the primary eigenvector that results in differential color coding on DTI. The MD images were used

to delineate the interfaces between parenchyma and the high-diffusivity cerebrospinal fluid (CSF) (e.g., pial surface and ventricles) and to refine minor details of parenchyma.

2.3 | Regions of interest

We labeled 14 regions of interest (ROIs) across the developing fetal brain; 10 of these had bilateral representation (Figure 1).

Telencephalic wall: The telencephalic wall demonstrates alternating regions of high and low anisotropy, as described by Huang (2010).

- Cortical plate (CP): the outermost layer of the parenchyma, demonstrating high anisotropy and relatively low MD. The CSF outlines the outer margin (pial surface), which shows low FA and MD.
- Subplate (SP): a layer of low FA and intermediate diffusivity subjacent to the CP.
- Intermediate zone (IZ), subventricular zone (SVZ), and ventricular zone (VZ): the deepest layers of the telencephalic wall, demonstrating high anisotropy and low MD. Due to spatial resolution and tissue contrast, the boundaries between the IZ, SVZ, and VZ cannot be delineated.
- Ganglionic eminence (GE): high anisotropy and low diffusivity tissue located along the ventral aspect of the frontal horns of the lateral ventricles and extending along the ventricular margin of the medial temporal horns. Further delineation was aided in 3D with the cFA map that demonstrates a coherent architecture (Vasung et al., 2019; Wilkinson et al., 2017)

Deep white matter: The coherent nature of white matter pathways is clearly depicted on FA and other diffusion scalar maps (Khan et al., 2019).

- Internal capsule (IC): clearly delineated high anisotropy white matter bundle. We independently segmented the anterior (ALIC) and posterior limb (PLIC); the genu provided an anatomic boundary, and differential orientation of the principal eigenvector was apparent on cFA.
- Corpus callosum (CC): clearly delineated due to high anisotropy. The red color-coded voxels derived from the left-to-right direction of the primary eigenvector contributed to determining the lateral boundaries. Ventrally, it was bounded by the cavum septum pellucidum and anterior horns of the lateral ventricles. As previous studies have reported a different sequence of myelination of the CC subparts (Kinney et al., 1988; Zanin et al., 2011), we independently segmented the genu (GCC), body (BCC), and splenium (SCC).

Other supratentorial

- Hippocampus (Hp): high-FA, C-shaped structure, laterally bounded by the temporal horns of the lateral ventricles.

Deep gray nuclei

- Lentiform nucleus (Ln): a low FA region bounded laterally by the IZ/SVZ/VZ and medially by the IC.
- Thalamus (Th): low FA and intermediate diffusivity region bounded laterally by the PLIC and medially by the lateral ventricles.

Posterior fossa

- Brainstem: was segmented primarily in the MD maps where the surrounding CSF clearly demarcated the pial surface. In the superior-posterior aspect, the boundary was defined as the inferior aspect of the Th.

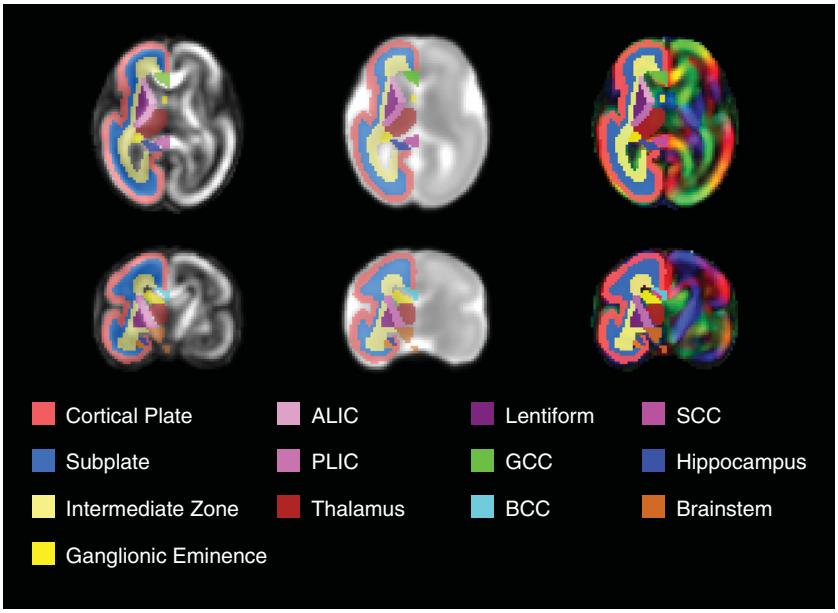

FIGURE 1 Tissue segmentation and structural labels overlaid on the right hemisphere of three diffusion-derived indices of the spatiotemporal fetal brain DTI atlas at week 26 of GA. Maps are left to right: Fractional anisotropy, mean diffusivity, and color-coded fractional anisotropy. ALIC, anterior limb of the internal capsule; PLIC, posterior limb of the internal capsule; GCC, genu of the corpus callosum; BCC, body of the corpus callosum; SCC, splenium of the corpus callosum

- Cerebellum: segmented primarily in the MD maps. It appeared as a low-MD structure anteriorly bounded by the brainstem and circumferentially by CSF.

2.4 | Statistical analysis

2.4.1 | Diffusion trends

The median FA and MD were calculated for each brain region with 25th–75th percentiles. A linear regression analysis was used to evaluate GA as a predictor of FA or MD, adjusting for laterality as a covariate. A logarithmic transformation was performed on the dependent variable (FA or MD), and the coefficients and confidence intervals (Cis) were converted using [exp(coefficient) − 1] × 100 to report the age-related change as a percentage.

2.5 | Label propagation

We performed a pilot analysis to investigate the reliability of propagating segmentations from the DTI atlas to individual subjects using a tensor-to-tensor registration algorithm. For performing this analysis, we obtained eight scans—one, subject for each GA week from 23 to 30—using the same inclusion criteria used in the atlas reconstruction and a similar protocol under HIPAA-compliant IRB-approved study. These subjects were separate from those used to create the atlas and were segmented in the same manner. The scans were reconstructed using the same method employed in the first step of the atlas reconstruction (Marami et al., 2017).

For the automatic segmentation, atlases closest to the subject's GA (t − 1, t, and $t + 1$) were registered to the subject using the tensor-based deformable registration algorithm in DTI-TK (Zhang et al., 2007); and FA and MD maps were estimated for the deformed atlases. The resultant warp field was then used to warp the labels from the atlas space to the subject space using ITK's generic label interpolator module (Schaerer et al., 2014). Subsequently, we used probabilistic STAPLE (Akhondi-Asl & Warfield, 2013) for multiple-template-based segmentation. In STAPLE, the segmentations and intensity map of the images are used to train a local Gaussian mixture model-based classifier. Then, the classifier is used to compute probabilistic segmentations of the target image, which are then fused.

For quantitative evaluation of atlas-based segmentation, we performed automatic segmentations by providing STAPLE the MD and FA atlas independently and calculated the Sørensen–Dice index (SDI). We performed a third experiment to create a composite segmentation using a mixture of experts model (MD + FA); for this model, we segmented each structure based on the individual diffusivity map (MD or FA) that had the highest individual performance. To note, we treated all the CC and IC subparts as part of the same structure.

All calculations were performed in RStudio (version 2021.09.1) using a significance level of .05. We performed Holm-Bonferroni correction for multiple comparisons at a α of .05 for each DTI-derived scalar (MD and FA). Plots were designed using the ggplot2 package (version 3.3.5).

3 | RESULTS

All 14 ROIs were segmented on the DTI-based FA and MD atlases from 23 to 30 weeks of GA. Figure 1 illustrates the segmentations in two orthogonal planes overlaid on the FA, cFA, and MD volumes. The volume of each ROI is summarized in Table 2S.

3.1 | Diffusion analysis

There were significant GA-related changes in FA in the ALIC, PLIC, the Ln, cerebellum, CP, SP, and IZ/SVZ/IZ (Table 1). The greatest increase in FA was seen in the cerebellum, and the largest decrease was seen in the SP. Figure 2 summarizes age-related changes in FA with age. The FA value of each ROI is summarized in Table 3S.

We also observed significant GA-related changes in MD in the brainstem, CP, CC, SP, ALIC, PLIC, IZ/SvZ/IZ, and GE (Table 2). The greatest increase was present in the GE; there was no significant GA-related decrease in MD for any of the ROIs. Figure 3 summarizes age-related changes in MD with age. The MD value of each ROI is summarized in Table 4S.

Of the structures with bilateral representation, only the hippocampus had a significant difference in FA based on laterality.

3.2 | Automatic segmentation

For most structures, the SDI coefficients exceeded 0.7. Table 3 shows the average SDI metrics for different structures; performance was similar when providing STAPLE the MD or FA maps. The structures with the lowest SDIs included small or narrow structures, including the CC, Hp, and IC, and inconspicuous structures, such as the GE. Figure 4 shows the result of the automatic segmentation of a 30-week subject when providing STAPLE the MD map.

4 | DISCUSSION

The development of robust motion correction algorithms for fetal brain DTI (Marami et al., 2017) overcame a major impediment for acquiring single-subject high-quality data and enabled previously unattainable analyses (Jaimes et al., 2020; Machado-Rivas et al., 2021). Among these, the creation of high-resolution spatiotemporal atlases of fetal brain DTI represents a tremendous leap forward (Khan et al., 2019). Our work presents a set of expertly segmented neuroanatomical labels for a fetal brain DTI atlas from 23 to 30 weeks of GA. Our labels address major limitations to the existing processing pipelines, including the changing contrast of the fetal brain, the presence of transient zones in the cerebral white matter, the small size of

TABLE 1 Fractional anisotropy values and change per gestational week

Structure	Median FA [range]	% change (95% CI)	p^a
Whole brain	0.12 [0.09–0.15]	−6.18 (−7.01 to −5.35)	**.001**
Telencephalic wall			
Cortical plate	0.14 [0.10–0.17]	−6.05 (−7.65 to −4.42)	**.001**
Subplate	0.10 [0.08–0.14]	−7.84 (−9.07 to −6.59)	**.001**
Intermediate zone	0.10 [0.09–0.14]	−5.17 (−6.36 to −3.97)	**.001**
Ganglionic eminence	0.14 [0.13–0.15]	−1.43 (−2.11 to −0.75)	**.001**
Deep white matter			
ALIC	0.12 [0.10–0.15]	−2.6 (−4.7 to −0.45)	.03
PLIC	0.18 [0.17–0.20]	1.54 (0.72–2.37)	**.002**
Corpus callosum			
Genu	0.26 [0.25–0.27]	1.15 (−0.1 to 2.41)	.07
Body	0.21 [0.18–0.23]	−2.33 (−4 to −0.64)	.02
Splenium	0.25 [0.24–0.27]	1.33 (0.73–1.94)	**.002**
Other supratentorial			
Hippocampus	0.11 [0.10–0.12]	−2.12 (−2.72 to −1.51)	**.001**
Deep gray nuclei			
Lentiform	0.11 [0.10–0.11]	−0.59 (−1.74 to 0.56)	.29
Thalamus	0.11 [0.09–0.12]	0.91 (−0.44 to 2.28)	.18
Posterior Fossa			
Brainstem	0.12 [0.11–0.13]	−1.61 (−3.65 to 0.47)	.11
Cerebellum	0.06 [0.05–0.08]	3.54 (1.31–5.81)	**.005**

Abbreviations: ALIC, anterior limb of the internal capsule; PLIC, posterior limb of the internal capsule.
[a]Listed in boldface when statistically significant after Holm-Bonferroni correction for multiple comparisons at an $\alpha < .05$.

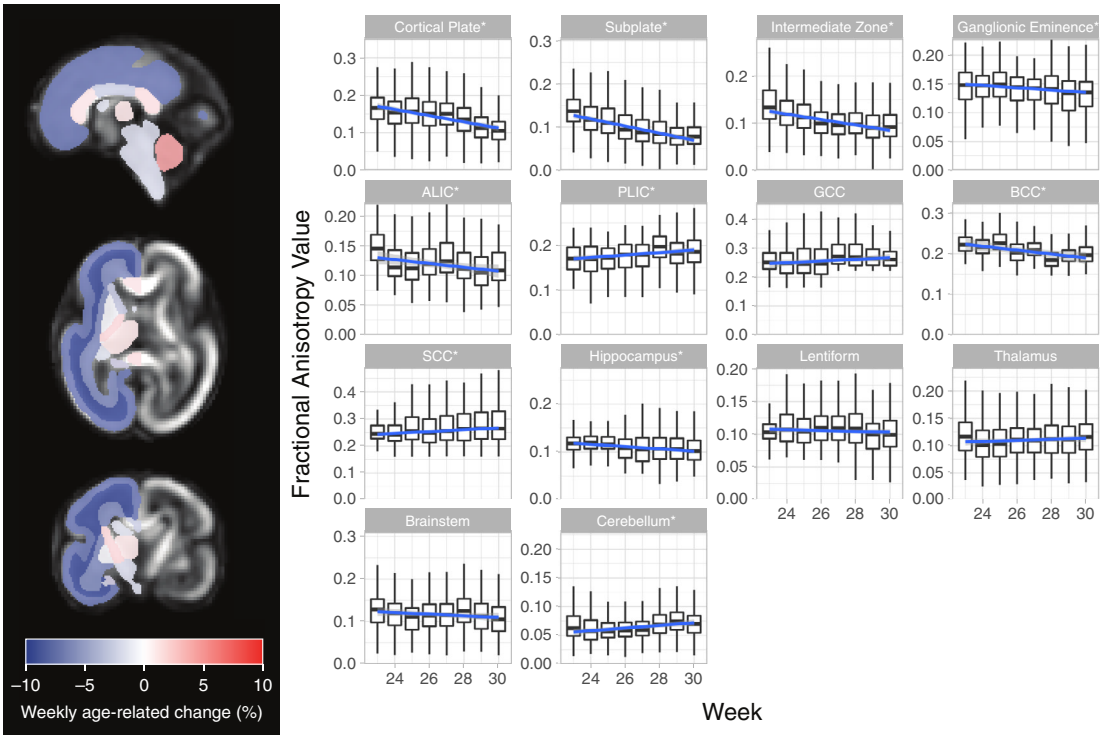

FIGURE 2 Left pane: Heatmap shows fractional anisotropy (FA) age-related change. Weekly age-related change is overlaid in the FA map of the 26-week-old atlas. Right pane: Boxplots depicting the distribution of FA values of each region of interest (ROI) at each gestational age. For each ROI, a linear model was fitted using the median ROI FA value as the dependent variable and gestational age as the independent variable. "*" represents that the model for that specific ROI was statistically significant at $p < .05$. ALIC, anterior limb of the internal capsule; PLIC, posterior limb of the internal capsule; GCC, genu of the corpus callosum; BCC, body of the corpus callosum; SCC, splenium of the corpus callosum

TABLE 2 Mean diffusivity values and change per gestational week

Structure	Median MD [range] ($\times 10^{-3}$ mm^2/s)	% change (95% CI)	p[a]
Whole brain	1.48 [1.41–1.54]	1.01 (0.64–1.37)	**.001**
Telencephalic wall			
Cortical plate	1.45 [1.40–1.51]	0.64 (0.35–0.92)	**.001**
Subplate	1.53 [1.43–1.60]	1.01 (0.61–1.42)	**.001**
Intermediate zone	1.51 [1.36–1.66]	2.26 (1.84–2.68)	**.001**
Ganglionic eminence	1.40 [1.21–1.57]	3.22 (2.55–3.9)	**.001**
Deep white matter			
ALIC	1.38 [1.23–1.45]	1.67 (0.99–2.35)	**.001**
PLIC	1.28 [1.24–1.33]	0.13 (−0.4 to 0.66)	.60
Corpus callosum			
Genu	1.39 [1.30–1.56]	2.18 (0.96–3.41)	**.005**
Body	1.48 [1.38–1.63]	2.08 (1.24–2.92)	**.001**
Splenium	1.48 [1.44–1.56]	0.78 (0.15–1.41)	.03
Other supratentorial			
Hippocampus	1.43 [1.37–1.52]	0.44 (−0.17 to 1.05)	.11
Deep gray nuclei			
Lentiform	1.36 [1.32–1.40]	−0.01 (−0.44 to 0.43)	.99
Thalamus	1.31 [1.27–1.38]	−0.37 (−0.91 to 0.17)	.16
Posterior Fossa			
Brainstem	1.31 [1.26–1.34]	0.07 (−0.81 to 0.96)	.95
Cerebellum	1.50 [1.43–1.63]	0.34 (−0.37 to 1.07)	.95

Abbreviations: ALIC, anterior limb of the internal capsule; PLIC, posterior limb of the internal capsule.
[a]Listed in boldface when statistically significant after Holm-Bonferroni correction for multiple comparisons at an $\alpha < .05$.

the brain, and immature sulcal pattern (Deshpande et al., 2015). Our study also provides an ROI-based evaluation of FA and MD changes utilizing the data from the atlas, which can aid in the clinical evaluation of fetal brain microstructure.

This study fills a critical gap by leveraging detailed labels in a robust spatiotemporal diffusion atlas constructed utilizing data from normally developing fetuses and focusing on a developmental stage that has been sparsely analyzed in the literature. The studies by Gupta et al., Huang et al., and Trivedi et al., provided insights into gross developmental changes in the microstructure of the fetal brain, albeit with a somewhat irregular sampling throughout the second half of gestation and utilizing ex vivo imaging (Gupta et al., 2005; Huang et al., 2009; Trivedi, Husain, et al., 2009). Additional information on microstructural development has been reported in cohorts of preterm infants (Batalle et al., 2019; Deipolyi et al., 2005; Hüppi et al., 1998; Maas et al., 2004; McKinstry, 2002). The general developmental trends described by these authors are in agreement with our work. Our approach expands on previous contributions by presenting in utero data devoid of potential confounders related to tissue handling/fixation of ex vivo specimens and prematurity-related injury and dysmaturation that could alter diffusion metrics (Batalle et al., 2017; Dimitrova et al., 2021; Kelly et al., 2016; Nosarti et al., 2014; Sun et al., 2005).

An important feature of the labels presented in our work is the emphasis on the laminar organization of the developing brain. During the second and early third trimesters, the telencephalic wall is arranged in a series of concentric zones (from outer to inner): the marginal zone (unapparent on MRI), the CP, SP, IZ, and the proliferative compartments (SVZ, VZ, GE) (Judaš et al., 2010; Rakic, 1982). Multiple authors have previously reported the differences in anisotropy and diffusivity in these zones (Maas et al., 2004; Trivedi, Husain, et al., 2009; Xu et al., 2014), and our 3D high-resolution atlases demonstrate these findings in exquisite detail. Unique histologic properties account for the appearance of the brain at this developmental stage on diffusion MRI (Kostovic, 2002; Zanin et al., 2011). Specifically, the high cellularity of the cortex and proliferative compartments results in low MD and high FA; the water-rich and relatively acellular SP has low FA and high MD; and the fibrillary IZ has high FA and intermediate MD (Huang et al., 2009). These tissue properties result in high tissue contrast between the transient zones of the fetal white matter, which often exceeds that obtained on single-shot T2-weighted images, particularly in the late second and early third trimesters. Other structures, particularly white matter structures with high-tissue coherence, are consistently identified on cFA maps throughout gestation (Machado-Rivas et al., 2021).

The developmental trends observed in our ROI analyses correlate well with prior observations. The decrease in FA and increase in MD in the fetal cortex are consistent with the results from McKinstry et al. and Trivedi et al., who described them in preterm infants and ex vivo specimens, respectively (McKinstry, 2002; Trivedi, Husain,

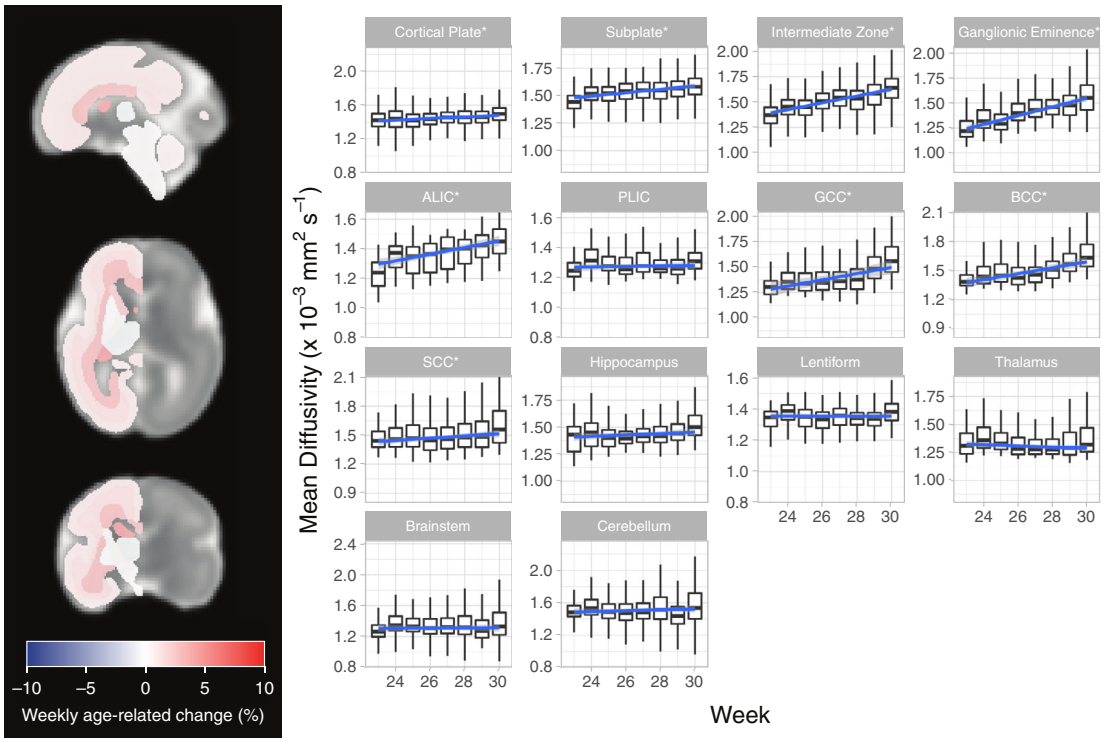

FIGURE 3 Left pane: Heatmap shows mean diffusivity (MD) age-related change. Weekly age-related change is overlaid in the MD map of the 26-week-old atlas. Right pane: Boxplots depicting the distribution of MD values of each region of interest (ROI) at each gestational age. For each ROI, a linear model was fitted using the median ROI MD value as the dependent variable and gestational age as the independent variable. "*" represents that the model for that specific ROI was statistically significant at $p < .05$. ALIC, anterior limb of the internal capsule; PLIC, posterior limb of the internal capsule; GCC, genu of the corpus callosum; BCC, body of the corpus callosum; SCC, splenium of the corpus callosum

et al., 2009). These changes have been attributed to dendritic arborization, synaptic formation, neuronal differentiation—which increase the extracellular space between neurons—and a decrease in glial fibrillary acid protein (McKinstry, 2002; Trivedi, Gupta, et al., 2009). Similar trends were also observed in the SP and IZ/SVZ/IZ, which are also consistent with the ex vivo data reported by Trivedi, Husain, et al. (2009) and Xu et al. (2014). Specifically, the major determinant of anisotropy in the fetal brain is the presence of the radial-glial fibers that guide neuronal progenitors from the germinal centers to their cortical targets; this radial glial scaffolding is known to decrease with age (Trivedi, Husain, et al., 2009; Xu et al., 2014). The changes in the deep white matter bundles, including the ALIC, PLIC, and CC, follow the expected developmental trajectories related to axonal re-organization, myelination gliosis, and myelination. In some cases, the patterns of GA-related change in FA and MD differ from results observed by other authors, occasionally appearing somewhat attenuated. This is the case of the GA-related decrease in FA in the BCC, which we attribute to volume averaging with the adjacent CSF in a segment of the CC that is particularly thin (posterior body and isthmus).

The study by Kahn and colleagues detailing the construction of the spatiotemporal atlas of fetal brain DTI also reported preliminary data on the FA and MD in major white matter pathways (Khan et al., 2019). Our work expands on this report by (1) performing a whole-brain segmentation inclusive of gray matter structures (cortical plate, deep gray nuclei) and posterior fossa structures, (2) providing 3D ROIs that encompass the entirety of the structures (e.g., the entire corpus callosum rather than a mid-sagittal slice), and (3) by labeling the transient white matter zones.

In addition to providing comprehensive and robust data derived from the normative atlas, our labels may be used for automated segmentation. We presented the results of a pilot analysis in a small cohort of normally developing fetuses with SDI values generally exceeding 0.7 when using the composite segmentation of the mixture of experts model. The modest SDIs reflect, at least in part, the small size of the structures analyzed. By virtue of the low volume of the fetal brain and its subcomponents, relatively minor segmentation errors result in high penalties in the SDI. This is illustrated by the GE, which is only a few voxels thick and, despite demonstrating high tissue contrast, showed the lowest SDI values. Low tissue contrast between other structures and limited spatial resolution are likely contributors. Future work will be aimed at improving the accuracy of automatic fetal DTI segmentation using multiple tissue contrasts (e.g., T1, T2, DTI) and/or deep learning and investigating various factors that could affect the quality of the segmentations, such as GA, motion during the scan, and spatial resolution.

Our study has several limitations. First, the accuracy of the labels is intrinsically limited by the spatial resolution and contrast of in utero diffusion MRI. Our study is unable to resolve small structures (e.g., amygdala or subthalamic nuclei) or the sublaminar architecture

TABLE 3 Average Sørensen–Dice coefficient for atlas-based automatic segmentation. Using fractional anisotropy and mean diffusivity maps as intensity maps in STAPLE, and the composite segmentation obtained in the mixture of experts model

	Mean SDI ± SD		
Structure	**FA map**	**MD map**	**Composite**
Whole brain	0.75 ± 0.17	0.75 ± 0.17	0.75 ± 0.17
Telencephalic wall			
Cortical plate	0.72 ± 0.19	0.73 ± 0.20	0.73 ± 0.19
Subplate	0.77 ± 0.16	0.76 ± 0.15	0.77 ± 0.16
Intermediate zone	0.78 ± 0.14	0.78 ± 0.14	0.78 ± 0.14
Ganglionic eminence	0.63 ± 0.17	0.64 ± 0.19	0.63 ± 0.19
Deep white matter			
Internal capsule	0.70 ± 0.22	0.68 ± 0.21	0.70 ± 0.22
Corpus callosum	0.70 ± 0.15	0.72 ± 0.15	0.72 ± 0.15
Other supratentorial			
Hippocampus	0.68 ± 0.15	0.69 ± 0.15	0.69 ± 0.15
Deep gray nuclei			
Lentiform	0.78 ± 0.17	0.78 ± 0.16	0.78 ± 0.17
Thalamus	0.81 ± 0.17	0.81 ± 0.17	0.81 ± 0.17
Posterior Fossa			
Brainstem	0.86 ± 0.06	0.87 ± 0.05	0.87 ± 0.05
Cerebellum	0.85 ± 0.08	0.86 ± 0.08	0.86 ± 0.08

Abbreviations: FA, fractional anistropy; MD, mean diffusivity; SDI, Sørensen–Dice index.

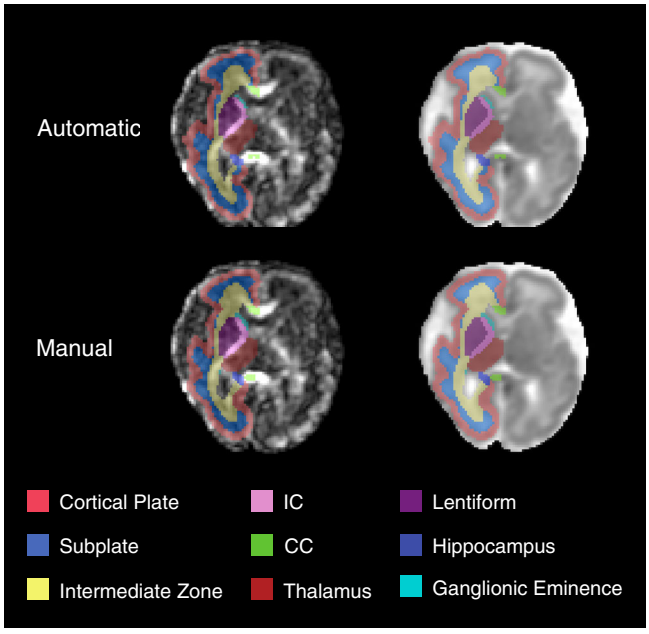

FIGURE 4 Comparison of automated segmentations and manual segmentations. Structural labels are overlaid on the right hemisphere of MD and FA maps in a 30-week-old fetus. The first row shows the results of the automatic segmentation, and the second row shows a manually segmented subject as a reference. CC, corpus callosum; IC, internal capsule

of various layers, including the cortex, SP, IZ, and proliferative compartments. This could result in volume averaging between neighboring layers such as the CP and superficial SP or the deep SP and IZ/SvZ/IZ (Gholipour et al., 2017). Second, we lack a histologic correlation for our labels. Our rigorous segmentations follow the tissue contrast of the atlases, but as the contrast decreases with GA, precise zonal differentiation becomes challenging (Bobić-Rasonja et al., 2021; Kostović et al., 2019; Pogledic et al., 2021). Finally, this work focused on a limited range of GAs; a comprehensive set of segmentations spanning the remainder of gestation would constitute an excellent resource for longitudinal studies. Future work should focus on improving and evaluating our robust atlas-to-subject registration algorithms and validating them in analyzing different cohorts of fetal subjects.

5 | CONCLUSION

In summary, this work introduced a set of expertly annotated neuroanatomical labels for a spatiotemporal atlas of fetal brain DTI and presented a pilot analysis of developmental changes in cerebral microstructure between 23 and 30 weeks of GA. Additional work is needed to improve algorithms that enable reliable label propagation to individual subjects and to utilize these for groupwise comparison between various populations.

FUNDING INFORMATION

The supported in part by the National Institute of Biomedical Imaging and Bioengineering, the National Institute of Neurological Disorders and Stroke, and Eunice Kennedy Shriver National Institute of Child Health and Human Development of the National Institutes of Health (NIH) under award numbers R01EB031849, R01NS106030, R01NS121657, R01EB018988, R01EB013248, R01EB032366, and R01HD109395; in part by the Office of the Director of the NIH under award number S10OD0250111; in part by a Technological Innovations in Neuroscience Award from the McKnight Foundation; and in part, this research was conducted with support from the Rosamund Stone Zander Translational Neuroscience Center, Boston Children's Hospital. C.J. was partly supported by the American Roentgen Ray Society scholarship and a career development award from the Office of Faculty Development at Boston Children's Hospital. The content of this publication is solely the responsibility of the authors and does not necessarily represent the official views of the NIH, the McKnight Foundation, the American Roentgen Ray Society, or the Boston Children's Hospital.

CONFLICT OF INTEREST

The authors have no conflicts of interest.

DATA AVAILABILITY STATEMENT

The data supporting the findings of this study are available on the Computational Radiology Laboratory webpage at http://crl.med.harvard.edu/research/fetal_brain_atlas/, reference number 1.

ORCID

Camilo Calixto https://orcid.org/0000-0001-5500-9721
Fedel Machado-Rivas https://orcid.org/0000-0003-3095-414X
Onur Afacan https://orcid.org/0000-0003-2112-3205
Camilo Jaimes https://orcid.org/0000-0002-7169-4244

REFERENCES

Akhondi-Asl, A., & Warfield, S. K. (2013). Simultaneous truth and performance level estimation through fusion of probabilistic segmentations. *IEEE Transactions on Medical Imaging*, *32*(10), 1840–1852.

Bastiani, M., Andersson, J. L. R., Cordero-Grande, L., Murgasova, M., Hutter, J., Price, A. N., Makropoulos, A., Fitzgibbon, S. P., Hughes, E., Rueckert, D., Victor, S., Rutherford, M., Edwards, A. D., Smith, S. M., Tournier, J.-D., Hajnal, J. V., Jbabdi, S., & Sotiropoulos, S. N. (2019). Automated processing pipeline for neonatal diffusion MRI in the developing human connectome project. *NeuroImage*, *185*, 750–763.

Batalle, D., Hughes, E. J., Zhang, H., Tournier, J. D., Tusor, N., Aljabar, P., Wali, L., Alexander, D. C., Hajnal, J. V., Nosarti, C., Edwards, A. D., & Counsell, S. J. (2017). Early development of structural networks and the impact of prematurity on brain connectivity. *NeuroImage*, *149*, 379–392.

Batalle, D., O'Muircheartaigh, J., Makropoulos, A., Kelly, C. J., Dimitrova, R., Hughes, E. J., Hajnal, J. V., Zhang, H., Alexander, D. C., Edwards, A. D., & Counsell, S. J. (2019). Different patterns of cortical maturation before and after 38 weeks gestational age demonstrated by diffusion MRI in vivo. *NeuroImage*, *185*, 764–775.

Bobić-Rasonja, M., Pogledić, I., Mitter, C., Štajduhar, A., Milković-Periša, M., Trnski, S., Bettelheim, D., Hainfellner, J. A., Judaš, M., Prayer, D., & Jovanov-Milošević, N. (2021). Developmental differences between the limbic and neocortical telencephalic wall: An intrasubject slice-matched 3T MRI-histological correlative study in humans. *Cerebral Cortex*, *31*(7), 3536–3550.

Deipolyi, A. R., Mukherjee, P., Gill, K., Henry, R. G., Partridge, S. C., Veeraraghavan, S., Jin, H., Lu, Y., Miller, S. P., Ferriero, D. M., Vigneron, D. B., & Barkovich, A. J. (2005). Comparing microstructural and macrostructural development of the cerebral cortex in premature newborns: Diffusion tensor imaging versus cortical gyration. *NeuroImage*, *27*(3), 579–586.

Deshpande, R., Chang, L., & Oishi, K. (2015). Construction and application of human neonatal DTI atlases. *Frontiers in Neuroanatomy*, *9*, 138. https://doi.org/10.3389/fnana.2015.00138/abstract

Dimitrova, R., Pietsch, M., Ciarrusta, J., Fitzgibbon, S. P., Williams, L. Z. J., Christiaens, D., Cordero-Grande, L., Batalle, D., Makropoulos, A., Schuh, A., Price, A. N., Hutter, J., Teixeira, R. P. A. G., Hughes, E., Chew, A., Falconer, S., Carney, O., Egloff, A., Tournier, J. D., … O'Muircheartaigh, J. (2021). Preterm birth alters the development of cortical microstructure and morphology at term-equivalent age. *NeuroImage*, *243*, 118488.

Feng, L., Li, H., Oishi, K., Mishra, V., Song, L., Peng, Q., Ouyang, M., Wang, J., Slinger, M., Jeon, T., Lee, L., Heyne, R., Chalak, L., Peng, Y., Liu, S., & Huang, H. (2019). Age-specific gray and white matter DTI atlas for human brain at 33, 36 and 39 postmenstrual weeks. *NeuroImage*, *185*, 685–698.

Gholipour, A., Rollins, C. K., Velasco-Annis, C., Ouaalam, A., Akhondi-Asl, A., Afacan, O., Ortinau, C. M., Clancy, S., Limperopoulos, C., Yang, E., Estroff, J. A., & Warfield, S. K. (2017). A normative spatiotemporal MRI atlas of the fetal brain for automatic segmentation and analysis of early brain growth. *Scientific Reports*, *7*(1), 476.

Gupta, R. K., Hasan, K. M., Trivedi, R., Pradhan, M., Das, V., Parikh, N. A., & Narayana, P. A. (2005). Diffusion tensor imaging of the developing human cerebrum. *Journal of Neuroscience Research*, *81*(2), 172–178.

Huang, H., Ceritoglu, C., Li, X., Qiu, A., Miller, M. I., van Zijl, P. C. M., & Mori, S. (2008). Correction of B0 susceptibility induced distortion in diffusion-weighted images using large-deformation diffeomorphic metric mapping. *Magnetic Resonance Imaging*, *26*(9), 1294–1302.

Huang, H., Xue, R., Zhang, J., Ren, T., Richards, L. J., Yarowsky, P., Miller, M. I., & Mori, S. (2009). Anatomical characterization of human fetal brain development with diffusion tensor magnetic resonance imaging. *The Journal of Neuroscience*, *29*(13), 4263–4273.

Huang, H. (2010). Structure of the fetal brain: What we are learning from diffusion tensor imaging. *The Neuroscientist*, *16*(6), 634–649.

Hüppi, P. S., Maier, S. E., Peled, S., Zientara, G. P., Barnes, P. D., Jolesz, F. A., & Volpe, J. J. (1998). Microstructural development of human newborn cerebral white matter assessed in vivo by diffusion tensor magnetic resonance imaging. *Pediatric Research*, *44*(4), 584–590.

Jaimes, C., Machado-Rivas, F., Afacan, O., Khan, S., Marami, B., Ortinau, C. M., Rollins, C. K., Velasco-Annis, C., Warfield, S. K., & Gholipour, A. (2020). In vivo characterization of emerging white matter microstructure in the fetal brain in the third trimester. *Human Brain Mapping*, *41*(12), 3177–3185.

Judaš, M., Sedmak, G., & Pletikos, M. (2010). Early history of subplate and interstitial neurons: From Theodor Meynert (1867) to the discovery of the subplate zone (1974): History of subplate zone and interstitial neurons. *Journal of Anatomy*, *217*(4), 344–367.

Kelly, C. E., Cheong, J. L. Y., Gabra Fam, L., Leemans, A., Seal, M. L., Doyle, L. W., Anderson, P. J., Spittle, A. J., & Thompson, D. K. (2016). Moderate and late preterm infants exhibit widespread brain white matter microstructure alterations at term-equivalent age relative to term-born controls. *Brain Imaging and Behavior*, *10*(1), 41–49.

Khan, S., Vasung, L., Marami, B., Rollins, C. K., Afacan, O., Ortinau, C. M., Yang, E., Warfield, S. K., & Gholipour, A. (2019). Fetal brain growth portrayed by a spatiotemporal diffusion tensor MRI atlas computed from in utero images. *NeuroImage*, *185*, 593–608.

Kinney, H. C., Brody, B. A., Kloman, A. S., & Gilles, F. H. (1988). Sequence of central nervous system myelination in human infancy. II. Patterns of myelination in autopsied infants. *Journal of Neuropathology and Experimental Neurology*, *47*(3), 217–234.

Kostovic, I. (2002). Laminar organization of the human fetal cerebrum revealed by histochemical markers and magnetic resonance imaging. *Cerebral Cortex*, *12*(5), 536–544.

Kostović, I., Sedmak, G., & Judaš, M. (2019). Neural histology and neurogenesis of the human fetal and infant brain. *NeuroImage*, *188*, 743–773.

Maas, L. C., Mukherjee, P., Carballido-Gamio, J., Veeraraghavan, S., Miller, S. P., Partridge, S. C., Henry, R. G., Barkovich, A. J., & Vigneron, D. B. (2004). Early laminar organization of the human cerebrum demonstrated with diffusion tensor imaging in extremely premature infants. *NeuroImage*, *22*(3), 1134–1140.

Machado-Rivas, F., Afacan, O., Khan, S., Marami, B., Velasco-Annis, C., Lidov, H., Warfield, S. K., Gholipour, A., & Jaimes, C. (2021). Spatiotemporal changes in diffusivity and anisotropy in fetal brain tractography. *Human Brain Mapping*, *42*(17), 5771–5784.

Manganaro, L., Bernardo, S., Antonelli, A., Vinci, V., Saldari, M., & Catalano, C. (2017). Fetal MRI of the central nervous system: State-of-the-art. *European Journal of Radiology*, *93*, 273–283.

Marami, B., Mohseni Salehi, S. S., Afacan, O., Scherrer, B., Rollins, C. K., Yang, E., Estroff, J. A., Warfield, S. K., & Gholipour, A. (2017). Temporal slice registration and robust diffusion-tensor reconstruction for improved fetal brain structural connectivity analysis. *NeuroImage*, *156*, 475–488.

McKinstry, R. C. (2002). Radial organization of developing preterm human cerebral cortex revealed by non-invasive water diffusion anisotropy MRI. *Cerebral Cortex*, *12*(12), 1237–1243.

Neil, J. J., Shiran, S. I., McKinstry, R. C., Schefft, G. L., Snyder, A. Z., Almli, C. R., Akbudak, E., Aronovitz, J. A., Miller, J. P., Lee, B. C., & Conturo, T. E. (1998). Normal brain in human newborns: Apparent

diffusion coefficient and diffusion anisotropy measured by using diffusion tensor MR imaging. *Radiology*, *209*(1), 57–66.

Nosarti, C., Nam, K. W., Walshe, M., Murray, R. M., Cuddy, M., Rifkin, L., & Allin, M. P. G. (2014). Preterm birth and structural brain alterations in early adulthood. *NeuroImage Clinical*, *6*, 180–191.

Oishi, K., Mori, S., Donohue, P. K., Ernst, T., Anderson, L., Buchthal, S., Faria, A., Jiang, H., Li, X., Miller, M. I., van Zijl, P. C. M., & Chang, L. (2011). Multi-contrast human neonatal brain atlas: Application to normal neonate development analysis. *NeuroImage*, *56*(1), 8–20.

Pogledic, I., Schwartz, E., Bobić-Rasonja, M., Mitter, C., Baltzer, P., Gruber, G. M., Milković-Periša, M., Haberler, C., Bettelheim, D., Kasprian, G., Judaš, M., Prayer, D., & Jovanov-Milošević, N. (2021). 3T MRI signal intensity profiles and thicknesses of transient zones in human fetal brain at mid-gestation. *European Journal of Paediatric Neurology*, *35*, 67–73.

Rakic, P. (1982). Early developmental events: Cell lineages, acquisition of neuronal positions, and areal and laminar development. *Neurosciences Research Program Bulletin*, *20*(4), 439–451.

Schaerer, J., Roche, F., & Belaroussi, B. (2014). A generic interpolator for multi-label images. *Insight Journal*. https://www.insight-journal.org/browse/publication/950

Sun, S. W., Neil, J. J., Liang, H. F., He, Y. Y., Schmidt, R. E., Hsu, C. Y., & Song, S.-K. (2005). Formalin fixation alters water diffusion coefficient magnitude but not anisotropy in infarcted brain. *Magnetic Resonance in Medicine*, *53*(6), 1447–1451.

Trivedi, R., Gupta, R. K., Husain, N., Rathore, R. K. S., Saksena, S., Srivastava, S., Malik, G. K., das, V., Pradhan, M., Sarma, M. K., Pandey, C. M., & Narayana, P. A. (2009). Region-specific maturation of cerebral cortex in human fetal brain: Diffusion tensor imaging and histology. *Neuroradiology*, *51*(9), 567–576.

Trivedi, R., Husain, N., Rathore, R. K. S., Saksena, S., Srivastava, S., Malik, G. K., das, V., Pradhan, M., Pandey, C. M., & Gupta, R. K. (2009). Correlation of diffusion tensor imaging with histology in the developing human frontal cerebrum. *Developmental Neuroscience*, *31*(6), 487–496.

Vasung, L., Charvet, C. J., Shiohama, T., Gagoski, B., Levman, J., & Takahashi, E. (2019). Ex vivo fetal brain MRI: Recent advances, challenges, and future directions. *NeuroImage*, *195*, 23–37.

Widjaja, E., Geibprasert, S., Mahmoodabadi, S. Z., Blaser, S., Brown, N. E., & Shannon, P. (2010). Alteration of human fetal subplate layer and intermediate zone during normal development on MR and diffusion tensor imaging. *American Journal of Neuroradiology*, *31*(6), 1091–1099.

Wilkinson, M., Kane, T., Wang, R., & Takahashi, E. (2017). Migration pathways of thalamic neurons and development of thalamocortical connections in humans revealed by diffusion MR tractography. *Cerebral Cortex (New York, NY: 1991)*, *27*(12), 5683–5695.

Woodward, L. J., Anderson, P. J., Austin, N. C., Howard, K., & Inder, T. E. (2006). Neonatal MRI to predict neurodevelopmental outcomes in preterm infants. *The New England Journal of Medicine*, *355*(7), 685–694.

Xu, G., Takahashi, E., Folkerth, R. D., Haynes, R. L., Volpe, J. J., Grant, P. E., & Kinney, H. C. (2014). Radial coherence of diffusion tractography in the cerebral white matter of the human fetus: Neuroanatomic insights. *Cerebral Cortex*, *24*(3), 579–592.

Zanin, E., Ranjeva, J., Confort-Gouny, S., Guye, M., Denis, D., Cozzone, P. J., & Girard, N. (2011). White matter maturation of normal human fetal brain. An in vivo diffusion tensor tractography study. *Brain and Behavior: A Cognitive Neuroscience Perspective*, *1*(2), 95–108.

Zhang, H., Avants, B. B., Yushkevich, P. A., Woo, J. H., Wang, S., McCluskey, L. F., Elman, L. B., Melhem, E. R., & Gee, J. C. (2007). High-dimensional spatial normalization of diffusion tensor images improves the detection of white matter differences: An example study using amyotrophic lateral sclerosis. *IEEE Transactions on Medical Imaging*, *26*(11), 1585–1597.

SUPPORTING INFORMATION

Additional supporting information can be found online in the Supporting Information section at the end of this article.

How to cite this article: Calixto, C., Machado-Rivas, F., Karimi, D., Cortes-Albornoz, M. C., Acosta-Buitrago, L. M., Gallo-Bernal, S., Afacan, O., Warfield, S. K., Gholipour, A., & Jaimes, C. (2023). Detailed anatomic segmentations of a fetal brain diffusion tensor imaging atlas between 23 and 30 weeks of gestation. *Human Brain Mapping*, *44*(4), 1593–1602. https://doi.org/10.1002/hbm.26160